Preparation and characterization of lithium–boron alloys: electrochemical studies as anodes in molten salt media, and comparison with pure lithium-involving systems

P. SANCHEZ*, C. BELIN
Laboratoire des Agrégats Moléculaires et Matériaux Inorganiques, U.A. C.N.R.S. 79, U.S.T.L. 2, Place Eugène Bataillon, 34060 Montpellier, Cedex, France

G. CREPY, A. DE GUIBERT‡
Laboratoires de Marcoussis, Route de Nozay, 91460 Marcoussis, France

Because of its low melting point (180.5 °C), lithium cannot be used as a negative electrode in high current density generators (particularly thermally activated batteries). The lithium–boron alloy, first discovered in 1978, presents advantageous properties: it remains solid and stable up to 650 °C and its electrochemical behaviour is very close to that of pure lithium. Conditions of synthesis of a metal lithium-rich alloy have been analysed; the multiphase material consisted of a porous refractory matrix filled with pure metal lithium, it was studied by nuclear magnetic resonance and its matrix examined by electron microscopy and porosimetry. Lithium–boron alloy electrochemical properties were analysed in LiCl–KCl media. In a flooded electrolyte, the behaviour of LiB is similar to that observed in non-aqueous media, particularly in dioxolane (DOL)–1.5 M $LiAsF_6$. In the case of single cell discharges (starved electrolyte), some problems arose from the nature of the electrolyte used (LiCl–KCl + SiO_2), which were solved by the substitution of SiO_2 by MgO in the electrolyte. Discharge curves were then identical to those obtained in flooded electrolytes and were characterized by two plateaux corresponding to the discharge of metallic lithium, and ionic lithium from the matrix, respectively.

1. Introduction

Earlier studies [1–9] have described the attractive properties of the lithium–boron alloy, first prepared by Wang [10], for use as anodes of thermal batteries operating at temperatures well above the melting point of lithium. Compared to lithium–aluminium anodes [11, 12], lithium–boron alloy presents better energy and power density characteristics. LiB shows excellent chemical behaviour, a potential close to that of pure lithium, and remains solid well above 600 °C. It is relatively malleable and can be shaped into thin foils, while Li–Al and Li–Si alloys are brittle powders that can be used only by pressing the powders into pellets and their potentials are largely below that of pure lithium [13–15]. In addition to the use of LiB in thermal batteries, its good specific capacity (1.93 Ah g^{-1}) makes it very attractive for use in high-energy non-aqueous batteries, occasionally operating at temperatures slightly above the melting point of lithium (180 °C).

The lithium–boron alloy is a two-phase system consisting of metallic lithium contained in a solid, ionic porous matrix [16, 17]. In a recent study of the

electrochemical behaviour of LiB in non-aqueous media at room temperature [18], extraction of lithium from the porous matrix was achieved with discharge efficiencies close to that of pure lithium, at current densities up to 10 mA cm^{-2}. LiB alloy samples with metallic lithium content from 43–52 wt % (corresponding to alloy samples with total lithium content between 66.5 and 72.0 wt %) were prepared. The importance of the metallic lithium content in the refractory matrix was demonstrated and correlated to the matrix porosity.

The practical use of lithium–boron alloys in batteries has been hindered hitherto by the difficulty in preparing large, homogeneous ingots. Owing to its exothermic, two-step mode of formation, the control of the LiB ingot structure is very difficult.

2. Experimental procedure

LiB alloys were prepared from lithium (99.94 wt %) and crystalline boron (99.5 wt %, 325 mesh), using the procedure already described [10, 19]. All the preparations were performed in a glove-bag filled with a

---

purified argon atmosphere (residual content of H_2O, N_2, O_2 less than 1 p.p.m.).

Differential scanning calorimetry (DSC) was performed using a "DSC 111 Setaram" microcalorimeter; samples were analysed in 110 mm³ stainless steel crucibles. The nuclear magnetic resonance (NMR) analysis of the allóy was performed on a "Brucker CXP 2000" spectrometer.
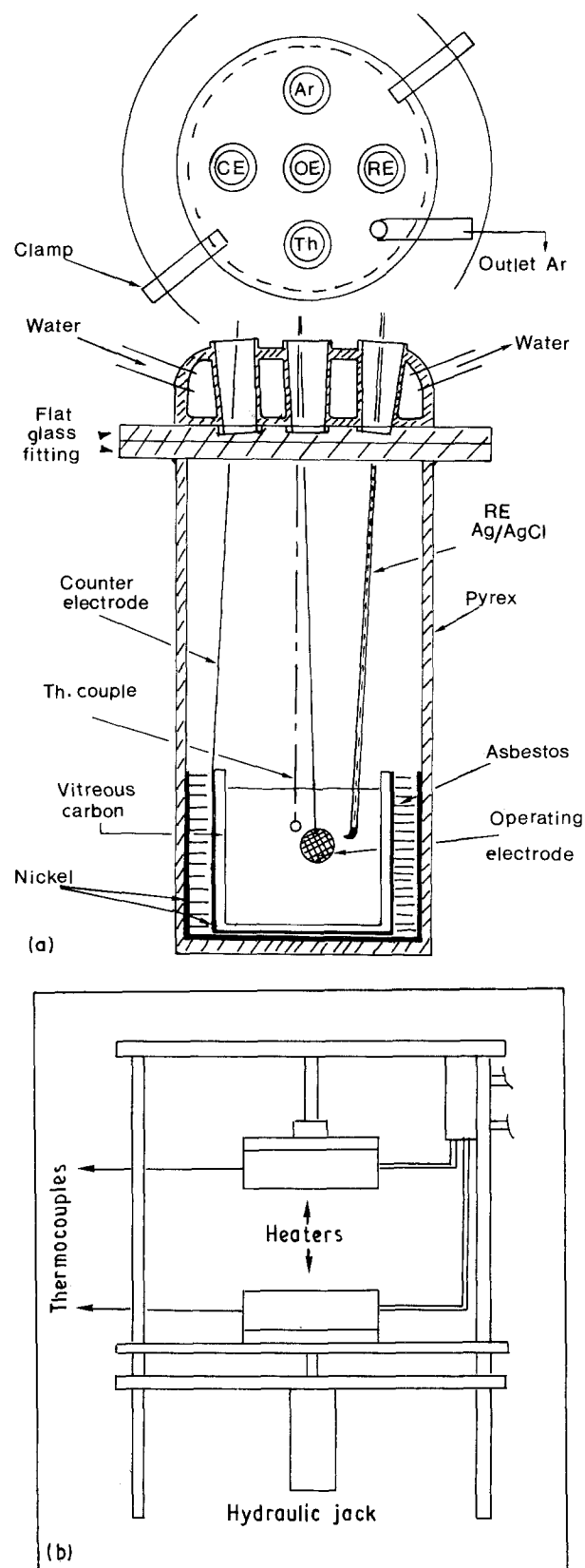

Figure 1 (a) Pyrex cell used for electrochemical studies of LiB in flooded electrolytes at 450 °C. (b) Experimental apparatus used for electrochemical studies of LiB in single cells.

The pure refractory ionic matrix was obtained after chemical extraction of the metal lithium by a solution of naphthalene in tetrahydrofuran and studied by electron microscopy and mercury porosimetry.

The Pyrex cell used for electrochemical studies in the flooded electrolyte (Fig. 1a) was filled with dried argon and its cover cooled by water circulation. The LiB alloy was pressed on to a nickel grid acting as current collector; the vitreous carbon counter-electrode contained the electrolyte which was the 45/55 wt % LiCl–KCl eutectic mixture. Single cell discharges were performed in the cell shown in Fig. 1b, where LiB anode discs, electrolyte (LiCl–KCl + SiO_2) and FeS_2 cathodic material pellets (18 mm diameter) were set between the two current collectors which could be heated at 450 °C. SiO_2, a gelling and binding agent, was added to the eutectic in order to provide a good mechanical strength to the electrolyte pellet.

3. Results and discussion

3.1. Preparation and characterization of the LiB alloy

In order to optimize the synthesis of the alloy (containing about 70 wt % Li), the reactivity of boron with lithium was studied by DSC. The reaction is characterized by two exothermic events (around 650 and 820 K), corresponding, as shown in Table I, to the formation of an intermediate compound (in this case $Li_{0.20}B$) and to the formation of the final refractory matrix (composition: $Li_{1.06}B$), respectively; the corresponding formation enthalpies are of the order of 3 and 9 kcal mol^{-1}. An alloy was then produced inside the glove-bag in an open reactor under continuous stirring at a heating rate of 4 °C min^{-1}. Samples were regularly taken out at the different stages of synthesis for analysis. For each sample an X-ray diffractogram was recorded; the remaining (unreacted) metallic lithium was determined by DSC and the total lithium content (Li$^+$ and Li^0) was determined by atomic absorption spectrometry. The results are given in Table II; it appears that the intermediate compound is obtained as an amorphous product, the final matrix begins to form at 440 °C but badly crystallizes in the first stages. This crystallization is accelerated in the last stages and leads to the solidification of the alloy at high temperature.

NMR study has shown that LiB is a two-phase material constituted of metallic lithium confined in an ionic refractory matrix (Fig. 2a). Subsequently, metallic lithium was extracted by a naphthalene–THF solution; the host matrix could then be studied by mercury-porosimetry and examined by electron microscopy. For a 66.5 wt % Li alloy, it was found that the matrix has an apparent density of 0.470 and a porosity of 0.671 associated with a mean pore radius of 1.5 μm, the porous and fibrous aspect of the matrix is shown well in Fig. 2b.

3.2. Discharges in the flooded electrolyte

3.2.1. Polarization determination

Linear potential sweep experiments allow, for an electron transfer reaction, the determination of the over-

TABLE I Results of the DSC study of the reactivity of lithium towards crystalline boron (325 mesh)

M_{total} (g)	Li (wt %)	First exothermic reaction			Second exothermic reaction		
		T (K)	$Li_{remaining}$ (wt %)	Intermediate product	T (K)	$Li_{remaining}$ (wt %)	Matrix composition
0.040 776	70.80	632	95.6	$Li_{0.166}B$	828	73.1	$Li_{1.016}B$
0.055 293	70.13	631	93.9	$Li_{0.223}B$	803	70.3	$Li_{1.086}B$
0.037 683	70.55	674	93.7	$Li_{0.235}B$	820	71.5	$Li_{1.063}B$
0.048 825	69.99	663	95.0	$Li_{0.182}B$	803	70.4	$Li_{1.075}B$
0.062 770	70.02	628	95.5	$Li_{0.236}B$	825	70.4	$Li_{1.059}B$

TABLE II Stages of preparation and characterization of a lithium–boron alloy using 11.16 g Li and 4.78 g B

Sampling	T (K)	Characteristics	Composition of products[a]	Evolution of characteristic X-ray lines of products: 2θ (deg)[b]					
				25.52	41.25	44.95	52.40	62.70	71.50
1	583	Lustreless grey liquid	$Li_{0.16}B$						
2	623	Slightly glossy liquid	$Li_{0.17}B$						
3	713	Shining viscous liquid	$Li_{0.23}B$	5.1	< 2	3.4			
4	743	Very viscous shining liquid	$Li_{0.29}B$	5.6	< 2	3.6			
5	753	Shining paste	$Li_{0.41}B$	6.8	< 2	4.1			
6	803	Start of solidification	$Li_{0.74}B$	36.0	3.2	23.0	< 2	< 2	< 2
7	843	End of reaction solid product	$Li_{1.08}B$	100	11.2	56.0	< 2	3.6	< 2

[a] Obtained by DSC (Li^0 content) and atomic absorption ($Li^0 + Li^+$ content).
[b] CuK_α.

potential sum ($E - E_0 = \Sigma \eta_1$) from the slope of the plot $I = f(E)$.

In Fig. 3, the polarization curves of the LiB electrode (10 mm diameter disc) and of several host structures impregnated with pure lithium are presented. These have been obtained in the LiCl–KCl eutectic at 450 °C. The corresponding numerical results, which are not corrected for the ohmic loss, are given in Table III.

The open circuit voltage for LiAl alloy is in agreement with that reported in the literature [20]. The host structures containing lithium behave differently according to the nature of the framework metal. The best result is obtained for the nickel structure; the porous nature of the LiB alloy gives the same advantages as a good host structure, this is corroborated by the similarity of the slopes of the $I = f(E)$ curves.

3.2.2. Cyclic voltammetry

Fig. 4 represents the cyclic voltammetry plot obtained for LiB in the LiCl–KCl electrolyte at 450 °C; the

TABLE III Slopes of $I = f(E)$ curves for different lithium host structures

Electrode	$E_{i=0}$ (V/Li)	$\delta E/\delta i$ (Ω cm^{-2})
Stainless steel structure	0	1.1
LiAl	0.360	1.0
LiB	0	0.7
Ni structure	0	0.65

polarization resistance was calculated using the micropolarization curve technique.

$R_{pol} = (\delta n/\delta i) = 0.2\ \Omega\text{cm}^2$ with the exchange current $i_0 = 325\ \text{mA cm}^{-2}$. These values can be compared with those obtained in the DOL–1.5 M LiAsF$_6$ electrolyte [18]: $R_{pol} = 37\ \Omega\text{cm}^2$ and $i_0 = 0.7\ \text{mA cm}^{-2}$. The former values evidently express the lowering of the energy barrier which is associated with the electron transfer.

3.2.3. Galvanostatic discharges

Galvanostatic discharges were performed at current densities ranging from 0.02–2 A cm^{-2}. The patterns of these curves are similar to those obtained with DOL–1.5 M LiAsF$_6$ [18]. They are represented (after correction of the ohmic loss) in Fig. 5. The two-phase nature of the electrode (metallic and ionic lithium) is suggested by the presence of two plateaux at low current density, as seen in Fig. 6. It should be noted that our interpretation of the poly-phase nature of the electrode is in contradiction with that given previously [1, 2]; whatever the initial lithium content, we have never observed the presence of solvated compounds such as $Li_2B \cdot xLi$ ($x = 1$, 2 or 4). At higher current density, the linear portion (AB) of the curve (Fig. 5) is characteristic of the effect of Li^+ ion diffusion from the electrode to the electrolyte; under these conditions, the concentration polarization term considerably increases and the reaction kinetics, while still controlled by electron transfer, is affected by the diffusion process. On the other hand, it is possible that both the
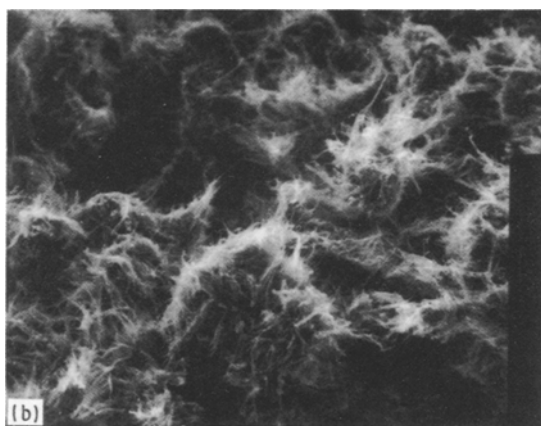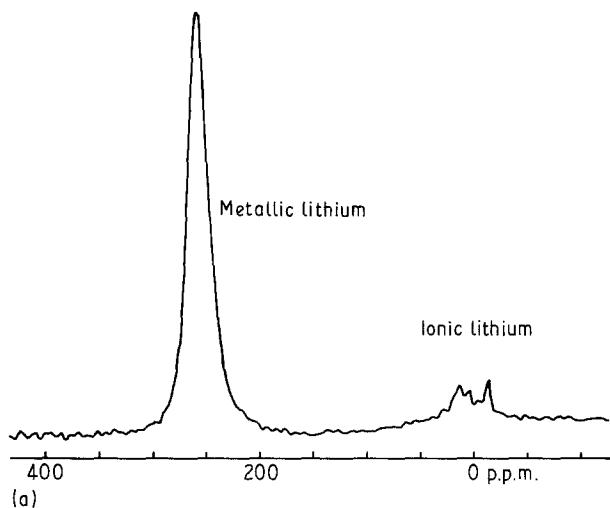
(a)

Figure 2 (a) ^{7}Li NMR spectrum of the lithium–boron alloy at 150°C. (b) Electron micrograph of the lithium–boron matrix (×650).
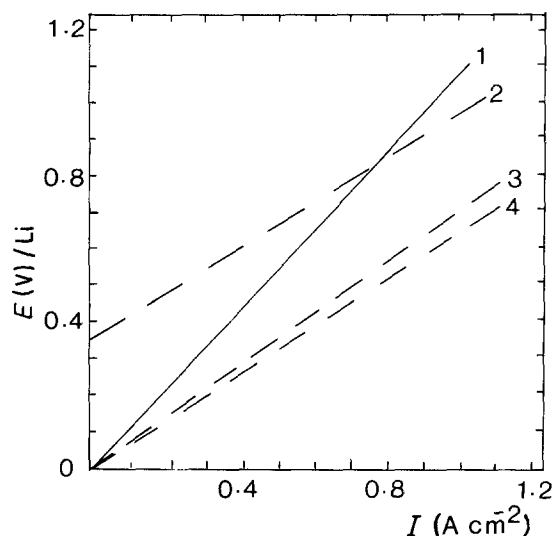

Figure 3 Polarization curves of several lithium host structures in LiCl–KCl eutectic electrolyte. (1) Stainless steel structure, (2) LiAl, (3) LiB, (4) nickel structure.

concentration polarization and the energy required to extract the lithium which is confined in the matrix pores, account for the gross polarization. This portion of the curve (AB) has not been reported by James and de Vries [1] even for a current density of 4 A cm^{-2}.
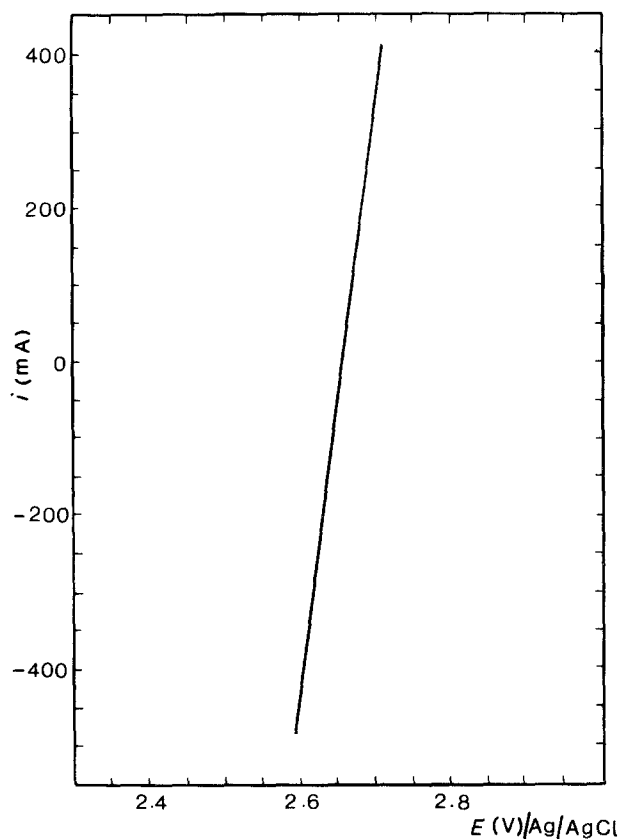

Figure 4 Micropolarization curve of the LiB electrode in LiCl–KCl electrolyte at 450°C.

The faradic efficiency ($R_f = \mathrm{Li_{extracted}}/\mathrm{Li_{extractable}}$) has been calculated for several LiB samples (Table IV), and they range from 70–80%. These variations are not very significant. James and de Vries [1] have shown that in the range 400–450°C, all the lithium is electrochemically collected; above 500°C some melted lithium can be lost by gravity and this phenomenon considerably increases at higher temperatures.

For the experimental conditions used in this work, it is clear that the faradic efficiency loss is not purely related to the loss of lithium by gravity, but rather to the kinetic competition between the two redox systems: $\mathrm{Li_{metal}}/\mathrm{Li^+}$ and $\mathrm{Li_{matrix}}/\mathrm{Li^+}$ whose discharge potentials are different. Tests have shown that under our experimental conditions, no more than 30% of the lithium forming the refractory matrix can be extracted; above this proportion the matrix decays and consequently the electrode is progressively consumed with loss of liquid lithium. If discharge conditions are not severe, and if less than 30% lithium has been extracted from the matrix at the end of discharge, only a mass of black material is observed on the nickel collector, which is similar to that which can be obtained after extraction of lithium from LiB alloys by a naphthalene–THF solution.

3.3. Single cell discharges

The first discharges in starved electrolytes gave results which were basically different from those obtained in

i (A cm^{-2})	m_{LiB} (mg)	η (mV)	$C_{discharged}$ (mA h)	$m_{Li^0\,extracted}$ (mg)	Li^0 extracted (%)	C (mAh mg$^{-1}_{Li^0(theo)}$)
0.02	17.0	10.0	18.8	4.9	70.3	2.7
0.1	20.0	30.0	22.0	5.8	70.7	2.7
0.2	19.0	60.0	19.8	5.2	66.7	2.5
0.5	19.0	100.0	22.9	6.0	76.9	2.9
1.0	19.0	200.0	27.9	7.3	76.8	2.9
2.0	20.0	350.0	25.0	6.5	79.6	3.0

flooded electrolyte experiments. Differences were observed between initial polarization, discharge times and general patterns. In Fig. 7 the discharge curves obtained in a flooded electrolyte and in a single cell are represented. Three points arise:

(i) in a single cell (open circuit), after 20 s, a loss of 200 mV is observed for the electrode potential while this potential is stable in flooded electrolytes;

(ii) at the beginning of discharge and for a current density of 100 mA cm^{-2}, the polarization is weaker (80 mV) in the case of flooded electrolytes than in single cells (600 mV);

(iii) in single cell discharges, several plateaux are observed. It is likely that in single cell discharges the nature of the electrolyte used can be at the origin of certain drawbacks: the SiO$_2$ which has been added to the eutectic as a gelling and binding agent, reacts very

quickly with lithium according to the reaction [21]

$$4Li(liq) + 3SiO_2 \rightarrow 2Li_2SiO_3(c) + Si(c) \quad (1)$$
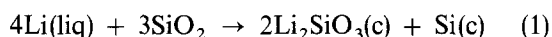
Probably silicon, in turn, can react with lithium to give Li$_x$Si compounds with different discharge potentials [22, 23]. In order to verify these facts, two tests were performed (Fig. 8).

1. The anode, the electrolyte (LiCl-KCl + SiO$_2$), and the cathode were inserted between current collectors and the open circuit voltage was recorded at 450 °C. It is observed that the potential decreases (polarization $\sim$ 600 mV) and then stabilizes after 70 s; this is characteristic of the instantaneous reactivity of lithium with SiO$_2$.

2. In the other experiment, a glass felt was intercalated between the anode and the electrolyte in order to avoid any contact between Li and SiO$_2$. This
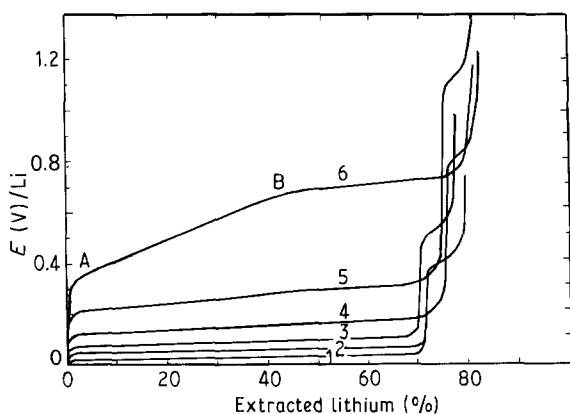

Figure 5 Galvanostatic discharges of LiB in flooded LiCl-KCl electrolyte at 450 °C at the different current densities of (1) 0.02, (2) 0.1, (3) 0.2, (4) 0.5, (5) 1 and (6) 2 A cm^{-2}.
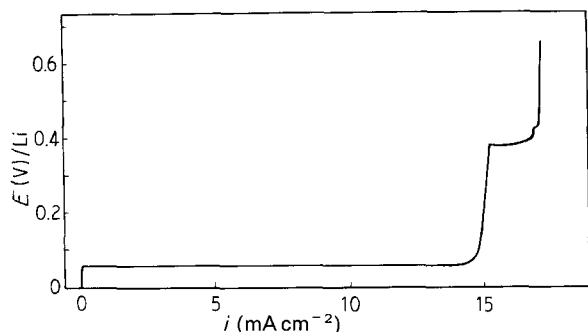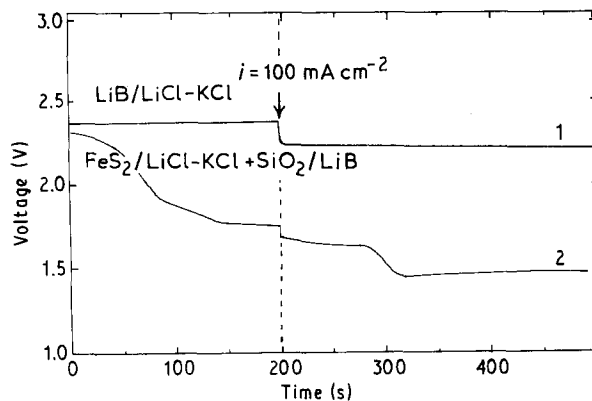

Figure 7 Evolution of the open circuit and discharge (i = 100 mA cm^{-2}) voltages of LiB as a function of time: (1) in flooded electrolyte, (2) in a single cell experiment.
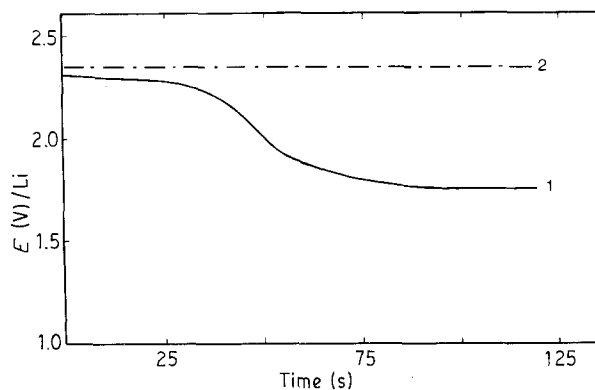

Figure 6 Galvanostatic discharge curve of LiB in LiCl-KCl at 450 °C and low current densities.

Figure 8 Stability study of the open circuit voltage of LiB in single cell: (1) against FeS$_2$/LiCl-KCl + SiO$_2$. (2) against FeS$_2$/LiCl-KCl + SiO$_2$/glass felt.
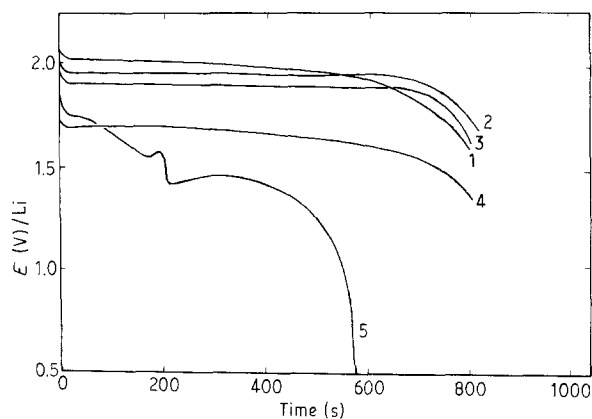
Figure 9 Single cell lithium discharges into FeS_2 in LiCl–KCl at 450 °C of the following electrodes: (1) Li in nickel foam, (2) LiB with artifice (glass felt + LiCl–KCl), corrected for the ohmic loss, (3) LiB with artifice (glass felt + LiCl–KCl), not corrected for the ohmic loss, (4) LiAl, (5) LiB without protection against SiO_2.

Figure 10 Single cell discharge curves at 450 °C of LiAl and LiB in LiCl–KCl (+ MgO).

procedure, as it can be seen in Curve 2 of Fig. 8, allowed the obtention of the same results as in flooded electrolytes; nevertheless the conducting properties of the stack (anode + glass felt + electrolyte + cathode) were seriously reduced. The intercalation of both a glass felt and a thin disc of the LiCl–KCl eutectic without SiO_2 between the anode and the LiCl–KCl/SiO_2 electrolyte offered the double advantage of isolating the anode from SiO_2 and of a better ionic conduction of the stack.

In Fig. 9, the discharge curves for different systems are shown; Curve 1 represents the discharge of a nickel foam impregnated with lithium, Curve 4 shows the discharge of the LiAl alloy and is characterized by a plateau at 1.7 V and a polarization of 360 mV versus pure lithium. Curve 5 (LiB/LiCl–KCl + SiO_2/FeS_2) is a typical example of discharge with severe drawbacks due to SiO_2. Curve 3 has been obtained by using the artifice (felt + LiCl–KCl eutectic); if corrected from the ohmic loss term (Curve 2), it becomes identical to that which is obtained in flooded electrolytes. It is worth noting that the intercalation of a glass felt and a LiCl–KCl disc doubles the electrolyte thickness; the internal resistance is 0.2 Ω, implying a polarization about 50 mV under an intensity of 255 mA.

On the other hand, disadvantages due to the reaction of lithium with SiO_2 can be overcome by replacing it with finely powdered MgO, in a proportion of 45 wt % in LiCl–KCl. The electrolyte, while still having a satisfactory mechanical strength, presents a good electrochemical behaviour. Fig. 10 clearly shows that LiB can advantageously replace LiAl in single cell discharges with a lower overpotential and a greater discharge efficiency.

4. Conclusion

The two-phase nature of the LiB alloy has been demonstrated by various techniques in order to understand better its electrochemical properties. In flooded molten salt electrolyte, LiB alloy behaves similarly as in non-aqueous organic media. The presence of two discharge plateaux confirms the two-
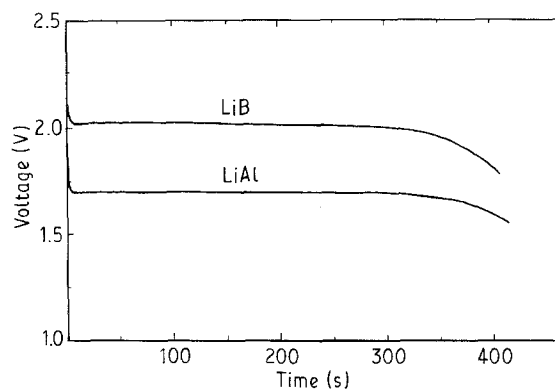
phase nature of the alloy. The intermediate compounds Li_2B and $Li_2B \cdot xLi$ ($x = 1$, 2 or 4) proposed by James and de Vries [1] have not been detected in this work.

In single cell discharges, silica used as gelling agent chemically reacts with LiB, but the resulting drawbacks can be overcome by the use of MgO instead of SiO_2. The results are then in good agreement with those obtained in flooded electrolyte and with those already reported [3, 5].

References

1. S. D. JAMES and L. E. DE VRIES, *J. Electrochem. Soc.* **123** (1976) 321.
2. L. E. DE VRIES, L. D. JACKSON and S. D. JAMES, *ibid.* **126** (1979) 993.
3. S. DALLEK, B. F. LARRICK and R. SZWARC, in 'Proceedings of 30th Power Sources Symposium", 7–12 June 1982 (The Electrochemical Society, 1982) p. 42.
4. R. SZWARC, R. D. WALTON, S. DALLEK and B. F. LARRICK, *J. Electrochem. Soc.* **129** (1982) 1168.
5. B. F. LARRICK, S. D. JAMES and R. SZWARC, in "Proceedings of the 28th Power Sources Symposium" (The Electrochemical Society, 1978) p. 95.
6. R. SZWARC and R. D. WALTON, NSWC/GEPP-TIS-451, Naval Surface Weapons Center, Silver Spring, MD, 31 March 1980.
7. S. D. JAMES, NSWC/TR-81-155, Naval Surface Weapons Center, Silver Spring, MD, April 1981.
8. S. D. JAMES, *J. Appl. Electrochem.* **12** (1982) 317.
9. R. SZWARC and S. DALLEK, NSWC/GEPP-TM-645, Naval Surface Weapons Center, Silver Spring, MD, May 1982.
10. F. E. WANG, US Pat. Appl. 4110111 (1978).
11. A. S. BARANSKI and W. R. FAWCETT, *J. Electrochem. Soc.* **129** (1982), 901.
12. I. EPELBOIN, M. FROMENT, M. GARREAU, J. THEVENIN and D. WARIN, *J. Electrochem. Soc.* **127** (1980) 2100.
13. C. J. WEN, B. A. BOUKAMP, R. A. HUGGINS and W. WEPPNER, *ibid.* **126** (1979) 2258.
14. R. N. SEEFURTH and R. A. SHARMA, *ibid.* **124** (1977) 1207.
15. S. DALLEK, D. W. ERNST and B. F. LARRICK, *ibid.* **126** (1979) 866.

16. D. W. ERNST, *ibid.* **129** (1982) 1513.
17. P. SANCHEZ and C. BELIN, *C.R. Acad. Sci. Paris* **307** série II (1988) 2027.
18. P. SANCHEZ, C. BELIN, G. CREPY and A. DE GUIBERT, *J. Appl. Electrochem.* **19** (1989) 421.
19. S. DALLEK, D. W. ERHST and B. F. LARRICK, *J. Electrochem. Soc.* **126** (1979) 866.
20. N. P. YAO, L. A. HEREDY and R. C. SAUNDERS, *ibid.* **118** (1971) 1039.
21. E. E. SCHUMACHER and W. C. ELLIS, *ibid.* **61** (1932) 91.
22. R. A. SHARMA and R. N. SEEFURTH, *ibid.* **123** (1976) 1763.
23. R. N. SEEFURTH and R. A. SHARMA, *ibid.* **127** (1980) 1101.